Development of photocatalytically active heterostructured MnO/ZnO and CuO/ZnO films via solution precursor plasma spray process

Zexin Yu, Hatem Moussa, Meimei Liu, Raphael Schneider, Weize Wang, Michel Moliere, Hanlin Liao

Development of ~~photocatalytic nanocomposite films with different compositional ratios and microstructures via a rapid one-step route~~ photocatalytically active heterostructured MnO/ZnO and CuO/ZnO films via a solution precursor plasma spray process

Zexin Yu[a]*, Hatem Moussa[b], Meimei Liu[a], Raphaël Schneider[b]*, Weize Wang[c], Michel Moliere[a], Hanlin Liao[a]

[a] *ICB UMR 6303, CNRS, site de UTBM, Université de Bourgogne Franche-Comté, 90010 Belfort, France*

[b] *Université de Lorraine, Laboratoire Réactions et Génie des Procédés (LRGP), UMR 7274, CNRS, 1 Rue Grandville, BP 20451, 54001 Nancy Cedex, France*

[c] *Key Lab of Safety Science of Pressurized System, Ministry of Education, School of Mechanical and Power Engineering, East China University of Science and Technology, 200237 Shanghai, China*

* *Corresponding author. E-mail address: zexin.yu@utbm.fr (Zexin Yu),*

raphael.schneider@univ-lorraine.fr (Raphaël Schneider).

~~Nanocomposite~~ Heterostructured ZnO photocatalysts for the degradation of organic pollutant are mainly synthesized by conventional chemical methods, suffering from long duration, multi-steps, and post-treatment of the powder-formed catalysts after usage. In this paper, Solution Precursor Plasma Spray (SPPS) process is demonstrated to be a fast and efficient method for the one-step preparation ~~of MnO/ZnO and CuO/ZnO nanocomposite films~~ of

MnO/ZnO and CuO/ZnO heterostructured films for photocatalytic applications. The ratios between MnO or CuO and ZnO materials in the films were easily adjusted by varying the molar ratio of $Mn(OAc)_2$ or $Cu(OAc)_2$ relative to $Zn(OAc)_2$ during the SPPS synthesis. To optimize the microstructure of selected CuO/ZnO films, two alternative spraying patterns were also developed. The modified films (Cu20-ZnO-A and Cu20-ZnO-B) were partly composed of nanorods (NRs) instead of conventional irregular particles. ~~All the MnO/ZnO and CuO/ZnO nanocomposite films~~ The MnO/ZnO and CuO/ZnO films exhibit narrower bandgap than pure ZnO films. ~~The photocatalytic performances of the ZnO based films were evaluated by the degradation of the Orange II dye under UV light or visible light irradiation.~~ The photocatalytic performances of the ZnO based films were evaluated for the degradation of the Orange II dye. Cu20-ZnO and Cu20-ZnO-B films exhibit the highest degradation efficiency under UV light and visible light, respectively. For example, the SPPS deposited Cu20/ZnO films could almost remove 90% of Orange II within 3 h ~~under~~ of UV light irradiation. Moreover, this study not only reveals that SPPS is of high potential for the ~~direct~~ deposition of ~~nanocomposite~~ heterostructured metal oxide films in rapid one-step, but also points out an efficient spraying strategy for adjusting the nanostructured morphologies in ~~nanocomposite films via SPPS route~~ these films.

***Keywords*:** Solution precursor plasma spray; ~~nanocomposite films~~ heterostructured films; microstructure; photocatalytic degradation

1. Introduction

The increasing amount of wastewater containing hazardous organic pollutants from various industries and the growing population are considered as one of the major threats to the surrounding ecosystem and to the health of human-beings [1]. Developing efficient and low-cost processes for purifying water from organic pollutants has been attempted through physical, chemical, biological and advanced oxidation processes (AOPs) [2]. One of the most promising AOP to remove contaminants from water is photocatalysis which is considered as a "green" technology as it requires only light and a catalyst [3-7]. Zinc oxide (ZnO) is one of most used semiconductor photocatalyst due to its availability, its low cost and its ability to degrade organic pollutants in wastewater (e.g. diazo dyes) under light irradiation [8-10]. However, the major limitation for the wide use of ZnO as photocatalyst is its activity limited to the UV region (bandgap of 3.37 eV), which accounts only for ca. 4% of the solar spectrum [11]. Moreover, ZnO suffers from a modest photocatalytic efficiency due to the easy recombination of the photogenerated-electron (e^-)-hole (h^+) pairs, which inhibits the generation of reactive oxygen species (ROS) like hydroxyl ($^{\bullet}OH$) or superoxide ($O_2^{\bullet-}$) radicals and H_2O_2 for the photodegradation reaction [12].

~~In order to make ZnO suitable for receiving and~~ To make ZnO suitable for utilizing solar energy and prevent charge recombination, coupling ZnO with semiconductors of lower bandgap, like CuO or MnO, has been reported [13-17]. This strategy is effective for extending the absorption range of ZnO to the visible light region but also to promote electron-hole pair separation and, consequently, achieve a higher photocatalytic activity. Recent studies demonstrated that ZnO coupled ~~by~~ with CuO or MnO exhibits improved performances compared to pure ZnO under UV or visible light irradiation for the degradation of some organic dyes [13-17]. ZnO nano-photocatalysts coupled by metal oxides are usually prepared by wet-chemical methods [14], precipitation methods [18] and hydrothermal methods [19], which suffer from multi-steps, long reaction times and low production efficiency ~~and thus inhibit the industrial promotion~~. Another important aspect is ~~that a filtration is required to~~ the reuse the nanoparticles, which may not only cause a loss of the catalyst but also a potential health risk [20-25]. The film-formed photocatalysts are a promising alternative to avoid these

drawbacks [20-25].

Thermal spray methods~~, exhibiting large production capacity and high efficiency with promising prospects~~ exhibit large production capacity, high efficiency, promising prospects from industrialization stand point [26-28], ~~have already been tried for~~ are of high potential for photocatalytic degradation applications [29-35]. Compared to other thermal spray methods (i.e. air plasma spray (APS) with powder, suspension plasma spray (SPS) and high velocity oxy-fuel spraying (HOVF)), ~~feasibility of controlling compositional ratio and complex composition in the nanocomposite films are the inherent advantages~~ the control of the films composition is the main advantages of Solution Precursor Plasma Spray (SPPS) process. The aforementioned advantages of SPPS can be attributed to the ~~usage of facial salt solutions~~ use of salt solutions as feedstock instead of solid powders mixtures, which are injected into a hot plasma plume going through a complex sequence of chemical and physical processes to form metal oxide films [36-39]. In the SPPS method, a direct-current plasma generated by a primary gas (e.g. argon) and a secondary gas (e.g. hydrogen) as the heat source is used to heat and accelerate the feeding solutions to deposit on the prepared substrates, which supply the direct formation of thin films in one-step [27, 36-38]. It should be noted that the duration of the preparation of photocatalytically active metal oxide films via SPPS is only several minutes. Similarly to the SPPS process, Spray Pyrolysis technology is another method for depositing films from solution precursors on preheated substrates [40]. Several photocatalytic films have been prepared by spray pyrolysis, such as ZnO [41-43], Al-doped ZnO [44, 45], Bi-doped ZnO [46] and ZnS films [47], etc. Due to the limited temperature of the heated substrate, there are some limitations for selecting solution precursors and using relative lower solution flow rate compared to the SPPS process. Although spray pyrolysis is a cheap and easy route, SPPS process with higher working temperature exhibits higher feasibility. However, the photodegradation efficiency is still the main limited aspect for the film-formed photocatalysts compared to that of powder-formed photocatalysts by the conventional methods [48-51]. ~~Generally, there is no doubt that film-formed photocatalysts would scarify the surface area of photocatalysts in the performance test, attributing as a primary reason for the limited performance. In addition, it has been commonly accepted that the microstructures of~~

~~photocatalysts, including size, crystal plane and nanostructured shapes, played crucial role in photocatalytic performance~~ It has been demonstrated that the microstructure of photocatalysts, including size, crystal orientation and shape, played a crucial role on the photocatalytic performances [52-55]. Compared to other conventional thermal spray method, the SPPS process exhibits higher ~~possibility~~ potential for the optimization of porous microstructure, forming smaller sized and well-shaped nanostructures owing to the use of precursor solutions rather than solid powder. To the best of our knowledge, studies related to the use of photocatalytically active MnO or CuO coupled to ZnO films prepared via a SPPS process have not yet been reported. Moreover, nanostructured morphologies (such as nanorods (NRs) and nanowires (NWs)) in the ~~nanocomposite~~ heterostructured metal oxide films by SPPS have never been described.

In this study, ~~nanocomposite~~ MnO/ZnO and CuO/ZnO films with different compositional ratio were prepared by the SPPS route using various spraying strategies and further used for the photocatalytic degradation of the Orange II dye under UV or visible light irradiation. The MnO/ZnO and CuO/ZnO films were characterized by scanning electron microscopy (SEM), X-ray diffraction (XRD) and Raman spectroscopy. UV-visible spectrophotometry (UV-vis) was also used to estimate the bandgap of MnO/ZnO and CuO/ZnO samples. Finally, for the CuO/ZnO sample, two modified spraying strategies were developed to form nanostructured morphologies in the thin films.

2. Experimental

2.1. Solution precursor preparation

Zinc acetate dihydrate ($Zn(OAc)_2 \cdot 2H_2O$, Alfa Aesar, ACS 98.0–101.0%), copper acetate monohydrate ($Cu(OAc)_2 \cdot H_2O$, Alfa Aesar, 98+%) and manganese acetate tetrahydrate ($Mn(OAc)_2 \cdot 4H_2O$, Alfa Aesar, Mn 22% (typical)) were chosen as precursors for the synthesis of ZnO, CuO and MnO, respectively. In order to explore the influence of MnO and CuO content in the MnO/ZnO and CuO/ZnO ~~nanocomposite~~ films, four precursor solutions were prepared by varying the $Mn(OAc)_2$:$Zn(OAc)_2$ and $Cu(OAc)_2$:$Zn(OAc)_2$ molar ratios, namely, 2.5:100, 5:100, 10:100 and 20:100. The concentration of $Zn(OAc)_2$ was kept constant as 0.2

M. The details of the solutions used are listed in Table 1. The pure ZnO film used as the reference sample was deposited from $Zn(OAc)_2$ to evaluate its photodegradation performance with MnO or CuO modified ZnO films.

2.2. Plasma spray conditions

A direct current (DC) plasma torch (F4, Oerlikon Metco, Switzerland) was used as heat source and attached to a six-axis robotic arm (ABB, Switzerland) for depositing the MnO/ZnO and CuO/ZnO films on commercial alumina plates (33 mm x 34 mm x 2 mm). The solution precursors were driven by the pressurized nitrogen flow through the stainless steel injector. In view of the different molar ratios in the feeding solutions, the samples are named as Mn2.5-ZnO, Mn5-ZnO, Mn10-ZnO and Mn20-ZnO as well as Cu2.5-ZnO, Cu5-ZnO, Cu10-ZnO and Cu20-ZnO (Table 1). In order to optimize the microstructure of Cu20-ZnO sample, two CuO/ZnO films with the same corresponding solution ratio were deposited by two modified spraying patterns. One modified ~~nanocomposite~~ CuO/ZnO film (called Cu20-ZnO-A) was prepared by injection of $Zn(OAc)_2$ and $Cu(OAc)_2$ solutions alternately in 4 cycles. The other modified CuO/ZnO film (named Cu20-ZnO-B) was prepared by firstly injecting the zinc solution, followed by the copper solution at the end. All other deposition parameters were kept the same. The schematic set-up for the SPPS process and corresponding injection strategies was illustrated in Fig. 1.

2.3. Characterization of the coatings

The surface morphologies of the MnO/ZnO, CuO/ZnO and reference ZnO films were examined by scanning electron microscopy (SEM, JEOL, JSM-5800LV). The compositions of the samples were determined by X-ray diffraction (XRD, Bruker AXS D8 focus, Germany) using a cobalt anticathode (λ = 1.78897 Å) with a scanning speed of 0.1 °/s. Raman spectra were recorded using an XploRA PLUS Raman Microscope (Horiba Jobin Yvon) with an excitation at 532 nm. UV-visible absorption spectra and diffuse reflectance spectra of MnO/ZnO and CuO/ZnO films were measured using a UV-vis spectrophotometer (Shimadzu, UV-2600). The bandgap values were estimated based on Kubelka-Munk equation by the Tauc

plots [56].

2.4. Photocatalytic testing

The photocatalytic performances of the MnO/ZnO, CuO/ZnO and reference ZnO films were evaluated by the degradation at room temperature of Orange II under the UV light irradiation produced by a Hg-Xe lamp. The activities of CuO/ZnO films were also investigated under visible light irradiation produced by a Xe lamp equipped with an ultraviolet cutoff filter ($\lambda >$ 420 nm). The light intensities were 15 mW/cm^2 for UV light and 7.5 mW/cm^2 for visible light. In a typical run, a set of five identical film pieces representing in total 60 mg of photocatalyst was placed into a Petri dish containing 60 mL of the Orange II aqueous solution (10 mg/L). Before irradiation, the liquid was magnetically stirred for 120 min in the dark to reach the adsorption-desorption equilibrium. During the subsequent light irradiation, 1 mL of the liquid was extracted at regular time intervals to evaluate the remaining concentration of Orange II by measuring its UV-visible absorption at 485 nm (Thermo Scientific Evolution 220 spectrophotometer). The photodegradation percentage of Orange II was calculated as follows:

$$D(\%) = \frac{C_0 - C_t}{C_0} \times 100\% \qquad Eq(1)$$

where C_0 is the initial concentration of Orange II and C_t is the concentration of Orange II after irradiation time t, respectively.

3. Results and discussions

3.1. Composition of the ~~nanocomposite~~ heterostructured films

The XRD patterns of the MnO/ZnO and CuO/ZnO films are shown in Fig. 2a-c. Due to the thin thickness of these films, the underlying alumina substrates (PDF 81-2267) are also detected in all the samples. The MnO/ZnO films only exhibit the XRD peaks of the standard hexagonal wurtzite structure of ZnO (PDF 75-0576) (Fig. 2a). MnO was not observed in these samples. However, the presence of MnO ~~in the films~~ could be detected by Raman spectroscopy (Fig. 3a). Similar with XRD patterns, the characteristic Raman peaks of the Al_2O_3 substrate (416, 644 and 746 cm^{-1}) were also observed [57]. The peaks located at 330,

378, 410 and 436 cm^{-1} can be assigned to E_2, A_{1TO}, E_1, and $E_{2\,(high)}$ vibration modes of ZnO with $P6_3mc$ symmetry, respectively [58]. The peaks at 317, 529 and 668 cm^{-1} are ascribed to MnO [59].

For the CuO/ZnO ~~nanocomposite~~ films with different compositional ratios, all diffraction peaks could be indexed to the standard hexagonal wurtzite structure of ZnO (PDF 75-0576) and CuO (PDF 74-1021) as well as to the underlying alumina substrates (PDF 81-2267) (Fig. 2b). The intensity of the CuO diffraction peaks ~~of CuO~~ increases with the $Cu(OAc)_2$ concentration in the feeding solution. The Raman spectra of the CuO/ZnO samples also exhibit the characteristic peaks of CuO at 289 and 627 cm^{-1} (Fig. 3b) [60].

The compositions of Cu20-ZnO-A and Cu20-ZnO-B samples prepared via the modified spraying methods were also analyzed by XRD and Raman spectroscopy. Owing to the high concentration of $Cu(OAc)_2$ in the raw solution precursors, the XRD peaks of the CuO phase (Fig. 2c) were more apparent than in the samples with low compositional ratio (Cu2.5-ZnO, Cu5-ZnO and Cu10-ZnO). The characteristic peaks of CuO (289 and 627 cm^{-1}) could also be observed in the Raman spectra as shown in Fig. 3c [60]. Moreover, it should be noted that the characteristic peak of single ZnO crystal at 340 cm^{-1} is more intense when using the modified spraying pattern (Fig. 3c) than when using the solution of mixed precursors. This may ascribed to the microstructure of the samples (*vide infra*) [61]. The XRD pattern of as-prepared reference ZnO films are shown in Fig. S1 and confirm the formation of the pure ZnO phase.

3.2. Microstructures of MnO/ZnO and CuO/ZnO films

The effect of the $Mn(OAc)_2/Zn(OAc)_2$ ratio in the feeding solution on the surface morphology of MnO/ZnO films was further investigated through SEM. It can be observed that the cauliflower-like microstructures gradually disappeared with the increase of the $Mn(OAc)_2$ concentration (Fig. 4a-d), which suggests a decrease of the surface area. The surface morphologies of CuO/ZnO films are shown in Fig. 4e-h. All the CuO/ZnO films also exhibited conventional cauliflower-like microstructures. Compared to MnO/ZnO composite, the compositional ratio between CuO and ZnO was found to be of less impact on the degree

of agglomeration of particles in the CuO/ZnO films compared to MnO/ZnO films.

The surface morphologies of two optimized CuO/ZnO films are shown in Fig. 4i-l. Cu20-ZnO-A and Cu20-ZnO-B samples are composed of NRs (marked with red rectangle) and irregular particles, which exhibited apparent different morphologies compared to the CuO/ZnO films using the mixture of solution precursors (Fig. 4e-h). EDS analyses further demonstrated that NRs-like particles were mainly composed by ZnO, while CuO is predominant in the irregular particles (Fig. S2 and Fig. S3). This result is consistent with Raman analyses (strong peak of ZnO at 340 cm^{-1} for Cu20-ZnO-A and Cu20-ZnO-B samples). For the Cu20-ZnO-A sample exhibiting sugar-coated haws-like microstructure, a close contact between CuO and ZnO particles can be seen. More separated NRs and irregular particles were observed in Cu20-ZnO-B films. Besides, more well-shaped ZnO NRs are obtained in Cu20-ZnO-B sample. In addition, the pure ZnO films exhibited classical cauliflower-like microstructure ~~as well~~ (Fig. S4), ~~which~~ and will be ~~employed as the comparative sample~~ used as reference.

As aforementioned ~~in the Introduction section~~, the SPPS process is similar to the spray pyrolysis technologies. It has been reported that nucleation from solution precursors occurs in the first stage ~~for the final formation of~~ when forming metal oxides [62]. ~~And our~~ Our previous study also ~~point~~ points out that that the formation of clusters from the zinc solution during the flight procedure is the precondition for obtaining ZnO nanostructures (i.e. NRs, NWs) via the SPPS route [63]. Firstly, for CuO-ZnO-A and Cu20-ZnO-B samples, due to the separated injection patterns, the nucleation of ~~desired cluster for~~ ZnO clusters is not ~~were less~~ affected by the copper solution. The ZnO NRs could be observed in the two films. For the Cu20-ZnO-B samples, ZnO ~~were separately~~ was deposited ~~with~~ within 12 cycles in prior to the deposition of CuO, ~~supporting~~ allowing more time for the nucleation and the growth of ZnO NRs ~~nanostructures~~. Therefore, more well-shaped NRs were observed (Fig. 4k-l). For

the other CuO/ZnO samples prepared from mixed solution, the coexistence of copper ~~salt~~ and zinc ~~salt~~ salts ~~would~~ influence the formation of ~~clusters of~~ ZnO clusters. This ~~point~~ result is agreement with previous ~~work~~ reports [64, 65]~~. Therefore,~~ and conventional cauliflower-like surface morphologies were observed instead (Fig. 4a-d and Fig. e-h).

Secondly, the CuO/ZnO and MnO/ZnO samples with different compositional ratios exhibit cauliflower-like microstructure with numerous irregular particles. ~~Because of~~ Due to the different ~~additional ratio~~ ratios of $Mn(OAc)_2$ or $Cu(OAc)_2$ in the ~~corresponding~~ precursor solutions, the density of solution, the supersaturation degree and ~~dimensional~~ the size of each solution droplet ~~should be~~ are different, ~~which could be attributed to~~ and this impacts the different microstructures of the films. ~~The effect of additional ratio on the microstructures was also found~~ Similar effects were observed in the spray pyrolysis method [44].

Thirdly, when comparing MnO/ZnO ~~films with~~ and CuO/ZnO samples prepared from mixture solutions, ~~less~~ a weaker agglomeration ~~degree~~ of particles ~~were~~ was observed (Fig. 4d). ~~Owing to the relative higher melting point of manganese acetate tetrahydrate (more than 300 ºC) compared to that of zinc acetate dihydrate (237 ºC), less energy would be left for the the assembly of particles to form unit cauliflower-like microstructure. This is similar to the effect of flow rate of hydrogen gas as mentioned in previous study [66]. Meanwhile, the melting point of copper acetate monohydrate is as low as 116 ºC, indicating more left available energy for agglomeration of particle in the copper zinc solutions compared to the manganese zinc solutions.~~ Due to the higher melting point of $Mn(OAc)_2$ (210°C) compared to $Cu(OAc)_2$ (116°C), less energy is available for the assembly of MnO/CuO particles into cauliflower-like microstructures compared to CuO/ZnO samples. This effect is similar to that of the hydrogen flow rate as mentioned in a previous study [66].

3.3. Optical properties of MnO/ZnO and CuO/ZnO films

The UV-visible absorption spectra of the films show that pure ZnO only absorbs UV light ($\lambda < 368$ nm) due to its wide bandgap (3.37 eV) [67]. XRD, Raman and SEM analyses show that MnO or CuO particles associated to ZnO are produced when using solution containing Zn^{2+} with Mn^{2+} or Cu^{2+} precursors. ~~Upon addition of MnO or CuO, the modified ZnO films~~ The heterostructured MnO/ZnO and CuO/ZnO films absorb in the visible region of the light spectrum ~~($\lambda > 400$ nm)~~ as shown in Fig. 5~~, which suggests that these materials should exhibit a photocatalytic activity under visible light irradiation~~. Moreover, the new chemical bonds generated by the heterojunction should favor the transfers of charge carriers between MnO or CuO and ZnO and thus increase the photocatalytic activity. The ~~corresponding~~ UV-visible diffuse reflectance spectra (DRS) of those films are gathered in Fig. S5. Using the Kubelka-Munk method [56], the corresponding bandgap (*Eg*) values were determined by extrapoling the plots at $(F(R) \times h\nu)^2 = 0$ (Fig. 6). MnO/ZnO and CuO/ZnO films exhibit a lower optical bandgap compared to pure ZnO films prepared by SPPS (3.12 eV) [39]. ~~For the CuO coupled ZnO photocatalysts, there is a p-n heterojunction/interface as illustrated in Fig. 7 [68-70]. For the ZnO, under light irradiation, the electrons were transferred from the 2p orbitals of O^{2-} (valence band, E_V) to $3d^{10}$ 4s orbitals of Zn^{2+} (conduction band, E_C) [71, 72]. For the CuO, the electrons were transferred from the 2p orbitals of O^{2-} (valence band) to $3d^9$ orbitals of Zn^{2+}, conduction band, E_C). The lower energy gap between O^{2-} (2p) and Cu^{2+} ($3d^9$) compared to that of O^{2-} (2p) and Zn^{2+} ($3d^{10}$ 4s) promote the absorption in the visible region. The narrowing bandgap should be attributed to the combined transitions from O2- (2p) to Zn2+ (3d10 4s) and to Cu2+ (3d9) [71, 72]. Secondly, as shown in the Fig. 7, there is bending of the conduction band (E_C) and valence band (E_V) at the interface, creating a novel equalization of the Fermi energy level (E_F) of the CuO and ZnO. A positively charged depletion layer is generated by the upward bending of bands in the n-type ZnO while a negatively charged accumulation layer is generated by the downward bending of bands in the p-type CuO [70, 73, 74]. And because of the difference of the band gaps of CuO and ZnO, the difference between the valence and conduction band at the interface is lower than that of ZnO. Thus, the generation of excitons in the CuO/ZnO could be triggered by visible light. Thirdly, in the the heterojunction, the creation of new chemical bonds between ZnO and CuO or MnO~~

~~could be expected [75].~~ For both MnO/ZnO and CuO/ZnO films, Eg was found to decrease ~~decreased~~ with the increase of MnO or CuO content in the photocatalysts ~~increment of compositional ratio between MnO or CuO with ZnO~~, which is agreement with previous studies [68-70]. Finally ~~Moreover~~, ~~the bandgap of films via SPPS process is~~ the bandgaps of the films were also sensitive to the injection patterns as shown in Fig. 6c~~, which indicate that mixture solution pattern could obtain a relative narrower bandgap~~. Using a mixture solution pattern allows to decrease the bandgap of the films. This likely originates from the increased ~~could be ascribed to the better~~ heterojunction between ZnO and CuO using the ~~from~~ mixture solution injection in the Cu20-ZnO sample ~~than that in~~ compared to the Cu20-ZnO-A and Cu20-ZnO ~~sample from~~ samples prepared via separated solution injection pattern.

3.4. Photodegradation performance under UV light

The photocatalytic activities of MnO/ZnO and CuO/ZnO films were first evaluated through the degradation of Orange II under UV light irradiation. Fig. 8 shown the plots of C_t/C_0 vs irradiation time, where C_0 and C_t are the initial concentration and the concentration at time t of the dye. The MnO- or CuO-modified ZnO samples exhibit better photodegradation performance than the pure ZnO films. For the MnO/ZnO samples, the photocatalytic performance decreased with the increase of MnO content in the catalysts ~~in the composite~~. ~~As previously discussed, the decrease in photocatalytic activity may be related to~~ This result may be linked to the decrease of the photocatalysts specific surface [39].

For the CuO/ZnO samples, the photodegradation efficiency is positively associated to the amount of CuO associated to ZnO. SEM images show that limited changes on the surface morphology were observed when varying the CuO:ZnO ratio compared to the MnO/ZnO films. Moreover, the CuO-modified ZnO samples exhibit better photodegradation performance than the MnO/ZnO samples. For example, the Cu20-ZnO films were able to remove 88% of Orange II within 3 h, while only 67% degradation was achieved by the Mn2.5-ZnO sample. Fig. 10c shows that both Cu20-ZnO-A and Cu20-Zn-B samples exhibit a slightly decrease activity compared to the Cu20-ZnO film (83% and 80% after 180 min irradiation, respectively). This result suggests that the simultaneous injection of $Zn(OAc)_2$ and

$Cu(OAc)_2$ is favorable for building a strong heterojunction between ZnO and CuO and thus for the decrease of the charge carriers recombination. In contrast, the separated injection pattern for the Cu20-ZnO-A and Cu20-ZnO-B samples seems to weaken the heterojunction between ZnO and CuO materials. ~~Fortunately, the Cu20-ZnO films via SPPS route exhibited relative favorably performance compared with the previous publications in Table 2 (increased photodegradation in shorter reaction times). Considering the SPPS method itself, it is also meaningful to further compare the performance with the previous photodegradation study based on thermal spray methods, as listed in Table S1.~~ Table 2 summarizes the photodegradation performances of various CuO/ZnO catalysts prepared through wet-chemical methods. The Cu20-ZnO films prepared via the SPPS route exhibit good performances compared to previous reports. Considering the SPPS method, it is also of interest to compare the performance of the films with those prepared via other thermal spray methods (Table S1). Our Cu20-ZnO films also exhibited improved degradation efficiency, which could be due to the advantages of SPPS process and good microstructures of our films.

The ~~photocatalytic kinetic of those~~ kinetics of the photocatalytic degradations mediated by CuO/ZnO films were also evaluated ~~in further step~~. ~~Fig. 9 illustrated the~~ The plots of $\ln(C_0/C_t)$ demonstrate a linear relationship with the irradiation time (Fig. 9), indicating that the photodegradation of Orange II at the surface of MnO/ZnO and CuO/ZnO films occurs following a pseudo-first-order reaction [71]

$$\ln\left(\frac{C_0}{C_t}\right) = k_{app}t \qquad Eq(2)$$

where k_{app} is the pseudo-first-order rate constant (min^{-1}). The improved reaction rate constants from MnO or CuO modified ZnO samples were also ~~confirmed compared with~~ compared to the pure ZnO film. ~~And the photocatalytic kinetic of MnO/ZnO films is negatively related to the additional concentration of $Mn(OAc)_2$ in original solution, while it displayed a positive correction with the additional concentration of $Cu(OAc)_2$ in the CuO/ZnO films.~~ The kinetics of the photocatalytic degradation of Orange II decrease when increasing the concentration of $Mn(OAc)_2$ in precursors solution, while it increases when using $Cu(OAc)_2$. The Cu20-ZnO sample exhibited

highest reaction rate ~~as~~ (0.0104 min^{-1}) under UV light irradiation followed by the Cu20-ZnO-A and Cu20-ZnO-B photocatalysts ~~successively, which exhibited the same ranking order of their bandgap values~~.

3.5. Photocatalytic activity under visible light

The photocatalytic activity of Cu20-ZnO, Cu20-ZnO-A and Cu20-ZnO-B materials was also evaluated under visible light irradiation (Fig.10a). The highest degradation efficiency was observed for the Cu20-ZnO-B photocatalyst ~~sample~~ (37.2% of Orange II degradation after 360 min irradiation) ~~based on the equation (1)~~, followed by Cu20-ZnO and Cu20-ZnO-A ~~sample~~ samples with degradation ~~efficiency~~ efficiencies of 24.4% and 22.1%, respectively.

~~Fig.10b showed the plots of $ln(C_0/C_t)$ demonstrate a linear relationship with the irradiation time. It obviously confirmed that Cu20-ZnO-B sample exhibited much higher calculated reaction rate constants as $14.1E^{-4}$ min^{-1}, which could be attributed to its surface morphology.~~ The plots of $ln(C_0/C_t)$ vs time confirm that the Cu20-ZnO-B sample exhibits the highest photocatalytic activity ($k = 14.1\ 10^{-4}\ min^{-1}$), which is likely linked to its surface morphology. ~~As mentioned in the previous study, 1-D nanostructured ZnO (i.e. NRs and NWs) with feature of the anisotropy morphology was reported to promote the separation of photogenerated holes/ electrons in the photodegradation test~~ Indeed, 1-D nanostructured ZnO (i.e. NRs and NWs) promote the separation of photogenerated electron/hole pairs [72]. The existences of apparent NRs in Cu20-ZnO-B films were able to increase the utilization efficiency of the limited photogenerated holes/electrons from visible light irradiation. In comparison with Cu20-ZnO, the slight lower photodegradation kinetic in Cu20-ZnO-A sample could be ascribed to its larger bandgap. ~~In the further work, optimization of CuO/ZnO would be further conducted to obtain higher photodegradation performance under both UV and visible light.~~

~~3.5~~ 3.6. ~~Plausible mechanism of those nanocomposite films for the photodegradation of dyes~~ Photodegradation mechanism

The enhanced photocatalytic activity of MnO/ZnO and CuO/ZnO films originates from the heterojunction between MnO or CuO and ZnO. In light of former studies and taking CuO/ZnO films as example, the following mechanisms are involved in the dye degradation [49, 65, 73].

$$\mathrm{CuO/ZnO} + h\nu \rightarrow \mathrm{CuO}(h^+)/\mathrm{ZnO}(e^-) \quad (1)$$

$$\mathrm{ZnO}(e^-) + \mathrm{O_2} \rightarrow \mathrm{O_2^-} + \mathrm{ZnO} \quad (2)$$

$$\mathrm{CuO}(h^+) + \mathrm{H_2O} \rightarrow \cdot\mathrm{OH} + \mathrm{H^+} \quad (3)$$

$$\cdot\mathrm{OH} + \mathrm{Orange\ II} \rightarrow \mathrm{Degradation\ products} \quad (4)$$

~~Fig. 11 illustrated the schematic diagram of excitation and transfer of electrons and holes for CuO/ZnO nanocomposite films under irradiation of light~~. A schematic representation of charge transfers upon light excitation of CuO/ZnO heterostructured films is described in Fig. 10. Under UV light irradiation, both CuO and ZnO are excited. ~~Due to the higher position of conduction band and valence band of CuO than those of ZnO, the photogenerated electrons (e^-) will transfer from conduction band (CB) of CuO to that of ZnO while the photogenerated holes (h^+) will transfer from valence band of ZnO to that of CuO~~ These electrons react with O_2 to produce superoxide ($O_2^{\bullet-}$) radicals. Simultaneously, holes in the valence band (VB) of ZnO move to the VB of CuO and react with water to generate hydroxyl ($^{\bullet}OH$) radicals [15, 49, 65, 73]. ~~If photogenerated e^-/ h^+) could migrate to the surface of ZnO and CuO, the highly oxidizing hydroxyl radicals ($\cdot OH$) and superoxide radicals ($\cdot O_2^-$), which attribute to the oxidation of Orange II dye.~~ The highly oxidizing $^{\bullet}OH$ and $O_2^{\bullet-}$ radicals are responsible for the oxidation of the Orange II dye.

4. Conclusion

MnO/ZnO and CuO/ZnO ~~nanocomposite~~ films were successfully synthesized and deposited

by ~~such~~ a rapid and one-step Solution Precursor Plasma Spray (SPPS) method and used for photodegradation application. ~~The existences of additional MnO and CuO in nanocomposite heterostructured films were confirmed by the XRD test and Raman spectra~~. For both of MnO/ZnO and CuO/ZnO films ~~prepared~~ from ~~feeding~~ mixture solution precursors, ~~the classic~~ cauliflower-like microstructures composed ~~by~~ of irregular particles were observed~~, which could be especially affected by the compositional ratio of MnO~~. ~~After employing~~ When using separated injection pattern of solution precursors, ~~apparent nanorods like nanostructures could be formed~~ NRs-like nanostructures were formed in the Cu20-ZnO-A and Cu20-ZnO-B samples, which be attributed to the ~~limit~~ limiting effect of CuO on the nucleation and ~~crystallization~~ growth of ZnO ~~owing to relative lower compositional ratio per unit time~~. From the EDS analysis, the NRs particles were mainly composed ~~with~~ of ZnO and the irregular particles were predominantly composed ~~by~~ of CuO. ~~In the light of the UV-Vis spectra, it clearly demonstrated that the optical bandgap could be efficiently narrowed by coupling of MnO or CuO.~~ UV-vis absorption spectra show that the optical bandgap of ZnO is narrowed by coupling with MnO or CuO. The Cu20-ZnO sample allows almost ~~removed~~ 90% degradation of the Orange II dye under UV light irradiation within 3h. The Cu20-ZnO-B sample exhibited the highest photodegradation efficiency under visible light (26.8% within 6 h) ~~of 26.8% within 6h under visible light~~. This study highlights that SPPS is a valuable method for the deposition of heterostructured metal oxide. ~~In addition, this study reveals that SPPS as an alternative for direct deposition of various heterostructured nanocomposite metal oxide films (i.e. ZnO-TiO_2, WO3-TiO_2, WO_3-ZnO and etc.) by such a rapid (within several minutes) and one-step route compared to the orthodox multi-steps methods. Moreover, it is also the pioneer work to point out the possible spray patterns for obtaining nanostructured morphologies in the nanocomposite heterostructured films via SPPS method.~~

Acknowledgement

The authors gratefully appreciate to the support from the China Scholarship Council (Grant No. 201504490038).

References

[1] Z. Cai, Y. Sun, W. Liu, F. Pan, P. Sun, J. Fu, An overview of nanomaterials applied for removing dyes from wastewater, Environmental Science & Pollution Research International, 24 (2017) 15882-15904.

[2] S. Parsons, Advanced oxidation processes for water and wastewater treatment, IWA publishing, 2004.

[3] S. Ahmed, M.G. Rasul, W.N. Martens, R. Brown, M.A. Hashib, Advances in Heterogeneous Photocatalytic Degradation of Phenols and Dyes in Wastewater: A Review, Water, Air, & Soil Pollution, 215 (2010) 3-29.

[4] M.N. Chong, B. Jin, C.W. Chow, C. Saint, Recent developments in photocatalytic water treatment technology: a review, Water Res, 44 (2010) 2997-3027.

[5] K.M. Lee, C.W. Lai, K.S. Ngai, J.C. Juan, Recent developments of zinc oxide based photocatalyst in water treatment technology: A review, Water Res, 88 (2016) 428-448.

[6] S. Malato, P. Fernández-Ibáñez, M.I. Maldonado, J. Blanco, W. Gernjak, Decontamination and disinfection of water by solar photocatalysis: Recent overview and trends, Catalysis Today, 147 (2009) 1-59.

[7] A.Y. Shan, T.I.M. Ghazi, S.A. Rashid, Immobilisation of titanium dioxide onto supporting materials in heterogeneous photocatalysis: A review, Applied Catalysis A: General, 389 (2010) 1-8.

[8] P.K. Chen, G.J. Lee, S.H. Davies, S.J. Masten, R. Amutha, J.J. Wu, Hydrothermal synthesis of coral-like Au/ZnO catalyst and photocatalytic degradation of Orange II dye, Materials Research Bulletin, 48 (2013) 2375-2382.

[9] J. Lv, W. Gong, K. Huang, J. Zhu, F. Meng, X. Song, Z. Sun, Effect of annealing temperature on photocatalytic activity of ZnO thin films prepared by sol–gel method, Superlattices and Microstructures, 50 (2011) 98-106.

[10] J. Yu, X. Yu, Hydrothermal synthesis and photocatalytic activity of zinc oxide hollow spheres, Environ Sci Technol, 42 (2008) 4902-4907.

[11] R. Saravanan, S. Karthikeyan, V.K. Gupta, G. Sekaran, V. Narayanan, A. Stephen, Enhanced photocatalytic activity of ZnO/CuO nanocomposite for the degradation of textile dye on visible light illumination, Mater Sci Eng C Mater Biol Appl, 33 (2013) 91-98.

[12] F. Achouri, S. Corbel, L. Balan, K. Mozet, E. Girot, G. Medjahdi, M.B. Said, A. Ghrabi, R. Schneider, Porous Mn-doped ZnO nanoparticles for enhanced solar and visible light photocatalysis, Materials & Design, 101 (2016) 309-316.

[13] K. Mageshwari, D. Nataraj, T. Pal, R. Sathyamoorthy, J. Park, Improved photocatalytic activity of ZnO coupled CuO nanocomposites synthesized by reflux condensation method, Journal of Alloys and Compounds, 625 (2015) 362-370.

[14] P. Sathishkumar, R. Sweena, J.J. Wu, S. Anandan, Synthesis of CuO-ZnO nanophotocatalyst for visible light assisted degradation of a textile dye in aqueous solution, Chemical Engineering Journal, 171 (2011) 136-140.

[15] L. Xu, Y. Zhou, Z. Wu, G. Zheng, J. He, Y. Zhou, Improved photocatalytic activity of nanocrystalline ZnO by coupling with CuO, Journal of Physics and Chemistry of Solids, 106 (2017) 29-36.

[16] S. Vignesh, M. Sivakami, P. Muniyappan, J.K. Sundar, Mechanistic investigation of FeO/MnO/ZnO nanocomposites for UV light driven photocatalytic performance, (2017).

[17] D. Chen, H. Zhang, S. Hu, J. Li, Preparation and enhanced photoelectrochemical performance of coupled bicomponent ZnO-TiO_2 nanocomposites, The Journal of Physical Chemistry C, 112 (2008) 117-122.

[18] B. Li, Y. Wang, Facile synthesis and photocatalytic activity of ZnO-CuO nanocomposite, Superlattices and Microstructures, 47 (2010) 615-623.

[19] S. Harish, J. Archana, M. Sabarinathan, M. Navaneethan, K.D. Nisha, S. Ponnusamy, C. Muthamizhchelvan, H. Ikeda, D.K. Aswal, Y. Hayakawa, Controlled structural and compositional characteristic of visible light active ZnO/CuO photocatalyst for the degradation of organic pollutant, Applied Surface Science, 418 (2017) 103-112.

[20] N.K. Dey, M.J. Kim, K.-D. Kim, H.O. Seo, D. Kim, Y.D. Kim, D.C. Lim, K.H. Lee, Adsorption and photocatalytic degradation of methylene blue over TiO_2 films on carbon fiber prepared by atomic layer deposition, Journal of Molecular Catalysis A: Chemical, 337 (2011) 33-38.

[21] S. Dosta, M. Robotti, S. Garcia-Segura, E. Brillas, I.G. Cano, J.M. Guilemany, Influence of atmospheric plasma spraying on the solar photoelectro-catalytic properties of TiO_2 coatings, Applied Catalysis B: Environmental, 189 (2016) 151-159.

[22] C. Guillard, J. Disdier, C. Monnet, J. Dussaud, S. Malato, J. Blanco, M.I. Maldonado, J.-M. Herrmann, Solar efficiency of a new deposited titania photocatalyst: chlorophenol, pesticide and dye removal applications, Applied Catalysis B: Environmental, 46 (2003) 319-332.

[23] H.-J. Wang, Y.-Y. Sun, C.-F. Wang, Y. Cao, Controlled synthesis, cytotoxicity and photocatalytic comparison of ZnO films photocatalysts supported on aluminum matrix,

Chemical Engineering Journal, 198-199 (2012) 154-162.

[24] J.-J. Wu, C.-H. Tseng, Photocatalytic properties of nc-Au/ZnO nanorod composites, Applied Catalysis B: Environmental, 66 (2006) 51-57.

[25] Y. Xu, M. Shen, Fabrication of anatase-type TiO_2 films by reactive pulsed laser deposition for photocatalyst application, Journal of Materials Processing Technology, 202 (2008) 301-306.

[26] G. Bertolissi, C. Chazelas, G. Bolelli, L. Lusvarghi, M. Vardelle, A. Vardelle, Engineering the Microstructure of Solution Precursor Plasma-Sprayed Coatings, Journal of Thermal Spray Technology, 21 (2012) 1148-1162.

[27] P. Fauchais, R. Etchart-Salas, V. Rat, J.F. Coudert, N. Caron, K. Wittmann-Ténèze, Parameters Controlling Liquid Plasma Spraying: Solutions, Sols, or Suspensions, Journal of Thermal Spray Technology, 17 (2008) 31-59.

[28] P. Fauchais, G. Montavon, Latest Developments in Suspension and Liquid Precursor Thermal Spraying, Journal of Thermal Spray Technology, 19 (2009) 226-239.

[29] J. Huang, Y. Gong, Y. Liu, X. Suo, H. Li, Developing titania-hydroxyapatite-reduced graphene oxide nanocomposite coatings by liquid flame spray deposition for photocatalytic applications, Journal of the European Ceramic Society, 37 (2017) 3705-3711.

[30] P. Daram, C. Banjongprasert, W. Thongsuwan, S. Jiansirisomboon, Microstructure and photocatalytic activities of thermal sprayed titanium dioxide/carbon nanotubes composite coatings, Surface and Coatings Technology, 306 (2016) 290-294.

[31] O. Solonenko, Y. Ando, H. Nishiyama, D. Kindole, A. Smirnov, A. Golovin, S. Uehara, T. Nakajima, Synthesis of thick photocatalytic titania surface layers by solution plasma spraying

and subsequent treatment by pulsed laminar plasma jet, Surface and Coatings Technology, 333 (2018) 39-51.

[32] M.C. Bordes, M. Vicent, A. Moreno, R. Moreno, A. Borrell, M. Salvador, E. Sánchez, Microstructure and photocatalytic activity of APS coatings obtained from different TiO_2 nanopowders, Surface and Coatings Technology, 220 (2013) 179-186.

[33] A. Navidpour, Y. Kalantari, M. Salehi, H. Salimijazi, M. Amirnasr, M. Rismanchian, M.A. Siahkali, Plasma-Sprayed Photocatalytic Zinc Oxide Coatings, Journal of Thermal Spray Technology, 26 (2017) 717-727.

[34] X. Liu, K. Wen, C. Deng, K. Yang, C. Deng, M. Liu, K. Zhou, Nanostructured Photocatalytic TiO 2 Coating Deposited by Suspension Plasma Spraying with Different Injection Positions, Journal of Thermal Spray Technology, 27 (2018) 245-254.

[35] F.-L. Toma, L.-M. Berger, I. Shakhverdova, B. Leupolt, A. Potthoff, K. Oelschlägel, T. Meissner, J.A.I. Gomez, Y. de Miguel, Parameters influencing the photocatalytic activity of suspension-sprayed TiO_2 coatings, Journal of thermal spray technology, 23 (2014) 1037-1053.

[36] P. Fauchais, M. Vardelle, S. Goutier, A. Vardelle, Key Challenges and Opportunities in Suspension and Solution Plasma Spraying, Plasma Chemistry and Plasma Processing, 35 (2014) 511-525.

[37] A. Killinger, R. Gadow, G. Mauer, A. Guignard, R. Vaßen, D. Stöver, Review of New Developments in Suspension and Solution Precursor Thermal Spray Processes, Journal of Thermal Spray Technology, 20 (2011) 677-695.

[38] L. Pawlowski, Suspension and solution thermal spray coatings, Surface and Coatings Technology, 203 (2009) 2807-2829.

[39] Z. Yu, H. Moussa, M. Liu, R. Schneider, M. Moliere, H. Liao, Solution precursor plasma spray process as an alternative rapid one-step route for the development of hierarchical ZnO films for improved photocatalytic degradation, Ceramics International, 44 (2018) 2085-2092.

[40] J.B. Mooney, S.B. Radding, Spray pyrolysis processing, Annual review of materials science, 12 (1982) 81-101.

[41] N. Kaneva, I. Stambolova, V. Blaskov, Y. Dimitriev, A. Bojinova, C. Dushkin, A comparative study on the photocatalytic efficiency of ZnO thin films prepared by spray pyrolysis and sol–gel method, Surface and Coatings Technology, 207 (2012) 5-10.

[42] I. Stambolova, V. Blaskov, M. Shipochka, S. Vassilev, V. Petkova, A. Loukanov, Simple way for preparation of ZnO films by surfactant mediated spray pyrolysis, Materials Science and Engineering: B, 177 (2012) 1029-1037.

[43] D. Klauson, I. Gromyko, T. Dedova, N. Pronina, M. Krichevskaya, O. Budarnaja, I.O. Acik, O. Volobujeva, I. Sildos, K. Utt, Study on photocatalytic activity of ZnO nanoneedles, nanorods, pyramids and hierarchical structures obtained by spray pyrolysis method, Materials Science in Semiconductor Processing, 31 (2015) 315-324.

[44] M. Bizarro, High photocatalytic activity of ZnO and ZnO: Al nanostructured films deposited by spray pyrolysis, Applied Catalysis B: Environmental, 97 (2010) 198-203.

[45] M. Bizarro, A. Sánchez-Arzate, I. Garduno-Wilches, J. Alonso, A. Ortiz, Synthesis and characterization of ZnO and ZnO: Al by spray pyrolysis with high photocatalytic properties, Catalysis today, 166 (2011) 129-134.

[46] T.-Y. Lin, Y.-T. Hsu, W.-H. Lan, C.-J. Huang, L.-C. Chen, Y.-H. Huang, J.-C. Lin, K.-J. Chang, W.-J. Lin, K.-F. Huang, Photocatalytic study of Zinc Oxide with bismuth doping

prepared by spray pyrolysis, Advances in nano research, 3 (2015) 123-131.

[47] İ. Altın, İ. Polat, E. Bacaksız, M. Sökmen, ZnO and ZnS microrods coated on glass and photocatalytic activity, Applied Surface Science, 258 (2012) 4861-4865.

[48] J.H. Sun, S.Y. Dong, Y.K. Wang, S.P. Sun, Preparation and photocatalytic property of a novel dumbbell-shaped ZnO microcrystal photocatalyst, J Hazard Mater, 172 (2009) 1520-1526.

[49] P. Senthil Kumar, M. Selvakumar, S. Ganesh Babu, S. Induja, S. Karuthapandian, CuO/ZnO nanorods: An affordable efficient p-n heterojunction and morphology dependent photocatalytic activity against organic contaminants, Journal of Alloys and Compounds, 701 (2017) 562-573.

[50] F. Lu, W. Cai, Y. Zhang, ZnO Hierarchical Micro/Nanoarchitectures: Solvothermal Synthesis and Structurally Enhanced Photocatalytic Performance, Advanced Functional Materials, 18 (2008) 1047-1056.

[51] A. Martinez-de La Cruz, U.G. Perez, Photocatalytic properties of BiVO4 prepared by the co-precipitation method: Degradation of rhodamine B and possible reaction mechanisms under visible irradiation, Materials research bulletin, 45 (2010) 135-141.

[52] A. Mclaren, T. Valdes-Solis, G. Li, S.C. Tsang, Shape and size effects of ZnO nanocrystals on photocatalytic activity, Journal of the American Chemical Society, 131 (2009) 12540-12541.

[53] E.S. Jang, J.H. Won, S.J. Hwang, J.H. Choy, Fine tuning of the face orientation of ZnO crystals to optimize their photocatalytic activity, Advanced Materials, 18 (2006) 3309-3312.

[54] K. Lv, Q. Xiang, J. Yu, Effect of calcination temperature on morphology and

photocatalytic activity of anatase TiO2 nanosheets with exposed {0 0 1} facets, Applied Catalysis B: Environmental, 104 (2011) 275-281.

[55] H. Wang, C. Xie, W. Zhang, S. Cai, Z. Yang, Y. Gui, Comparison of dye degradation efficiency using ZnO powders with various size scales, Journal of Hazardous materials, 141 (2007) 645-652.

[56] A.E. Morales, E.S. Mora, U. Pal, Use of diffuse reflectance spectroscopy for optical characterization of un-supported nanostructures, Revista mexicana de física, 53 (2007) 18-22.

[57] P. Li, M. Lei, W. Tang, Raman and photoluminescence properties of α-Al_2O_3 microcones with hierarchical and repetitive superstructure, Materials Letters, 64 (2010) 161-163.

[58] J. Wang, Y. Xia, Y. Dong, R. Chen, L. Xiang, S. Komarneni, Defect-rich ZnO nanosheets of high surface area as an efficient visible-light photocatalyst, Applied Catalysis B: Environmental, 192 (2016) 8-16.

[59] K. Ramesh, L. Chen, F. Chen, Y. Liu, Z. Wang, Y.-F. Han, Re-investigating the CO oxidation mechanism over unsupported MnO, Mn_2O_3 and MnO_2 catalysts, Catalysis Today, 131 (2008) 477-482.

[60] M.H. Chou, S.B. Liu, C.Y. Huang, S.Y. Wu, C.L. Cheng, Confocal Raman spectroscopic mapping studies on a single CuO nanowire, Applied Surface Science, 254 (2008) 7539-7543.

[61] A. Umar, S.H. Kim, E.K. Suh, Y.B. Hahn, Ultraviolet-emitting javelin-like ZnO nanorods by thermal evaporation: Growth mechanism, structural and optical properties, Chemical Physics Letters, 440 (2007) 110-115.

[62] V.K. Jayaraman, A. Hernández-Gordillo, M. Bizarro, Importance of precursor type in fabricating ZnO thin films for photocatalytic applications, Materials Science in

Semiconductor Processing, 75 (2018) 36-42.

[63] Z. Yu, H. Moussa, M. Liu, B. Chouchene, R. Schneider, W. Wang, M. Moliere, H. Liao, Tunable morphologies of ZnO films via the solution precursor plasma spray process for improved photocatalytic degradation performance, Applied Surface Science, (2018).

[64] K. Jayanthi, S. Chawla, K. Sood, M. Chhibara, S. Singh, Dopant induced morphology changes in ZnO nanocrystals, Applied Surface Science, 255 (2009) 5869-5875.

[65] R. Saravanan, S. Karthikeyan, V. Gupta, G. Sekaran, V. Narayanan, A. Stephen, Enhanced photocatalytic activity of ZnO/CuO nanocomposite for the degradation of textile dye on visible light illumination, Materials Science and Engineering: C, 33 (2013) 91-98.

[66] C. Zhang, X. Geng, H. Li, P.-J. He, M.-P. Planche, H. Liao, M.-G. Olivier, M. Debliquy, Microstructure and gas sensing properties of solution precursor plasma-sprayed zinc oxide coatings, Materials Research Bulletin, 63 (2015) 67-71.

[67] A. Janotti, C.G. Van de Walle, Fundamentals of zinc oxide as a semiconductor, Reports on Progress in Physics, 72 (2009) 126501.

[68] M. Mansournia, L. Ghaderi, CuO@ ZnO core-shell nanocomposites: novel hydrothermal synthesis and enhancement in photocatalytic property, Journal of Alloys and Compounds, 691 (2017) 171-177.

[69] M.T. Qamar, M. Aslam, I.M. Ismail, N. Salah, A. Hameed, Synthesis, characterization, and sunlight mediated photocatalytic activity of CuO coated ZnO for the removal of nitrophenols, ACS applied materials & interfaces, 7 (2015) 8757-8769.

[70] P. Lu, W. Zhou, Y. Li, J. Wang, P. Wu, Abnormal room temperature ferromagnetism in CuO/ZnO nanocomposites via hydrothermal method, Applied Surface Science, 399 (2017)

396-402.

[71] J. Kaur, S. Bansal, S. Singhal, Photocatalytic degradation of methyl orange using ZnO nanopowders synthesized via thermal decomposition of oxalate precursor method, Physica B: Condensed Matter, 416 (2013) 33-38.

[72] X. Zhang, J. Qin, Y. Xue, P. Yu, B. Zhang, L. Wang, R. Liu, Effect of aspect ratio and surface defects on the photocatalytic activity of ZnO nanorods, Scientific reports, 4 (2014) 4596.

[73] S. Jung, K. Yong, Fabrication of CuO-ZnO nanowires on a stainless steel mesh for highly efficient photocatalytic applications, Chemical Communications, 47 (2011) 2643-2645.

[74] X.-Q. LI, Q.-F. FAN, G.-L. LI, Y.-H. HUANG, Z. GAO, X.-M. FAN, C.-L. ZHANG, Z.-W. ZHOU, Syntheses of ZnO nano-arrays and spike-shaped CuO/ZnO heterostructure, Acta Physico-Chimica Sinica, 31 (2015) 783-792.

[75] A. Wei, L. Xiong, L. Sun, Y.-J. Liu, W.-W. Li, CuO Nanoparticle Modified ZnO Nanorods with Improved Photocatalytic Activity, Chinese Physics Letters, 30 (2013) 046202.

[76] C. Yang, X. Cao, S. Wang, L. Zhang, F. Xiao, X. Su, J. Wang, Complex-directed hybridization of CuO/ZnO nanostructures and their gas sensing and photocatalytic properties, Ceramics International, 41 (2015) 1749-1756.

[77] Y. LIU, S. WEI, L. LIU, X. LI, J. SHI, Fabrication of ZnO/CuO Layer-Stacked Composite Films and Their Photocatalytic Activity, Journal of the Chinese Ceramic Society, 40 (2012) 402-407.

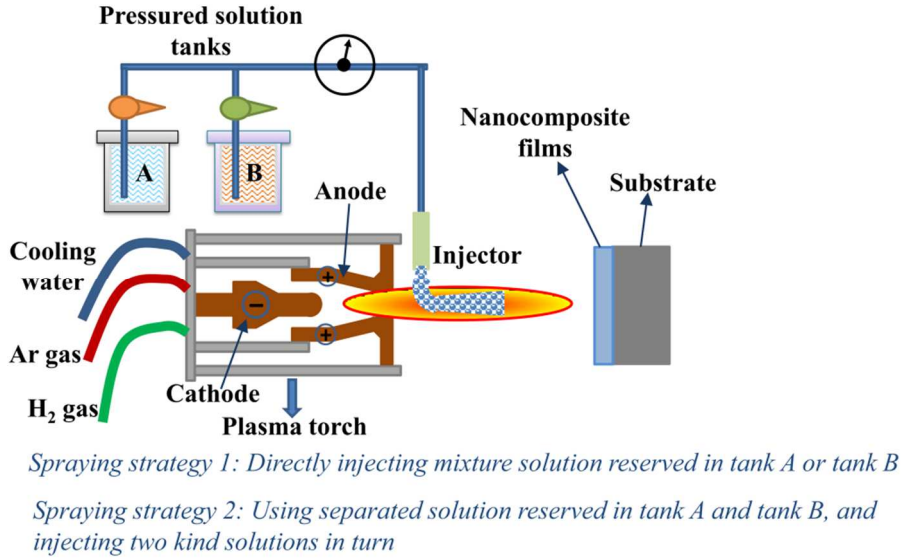

Fig. 1. Schematic representation of the SPPS process and of spraying strategies.

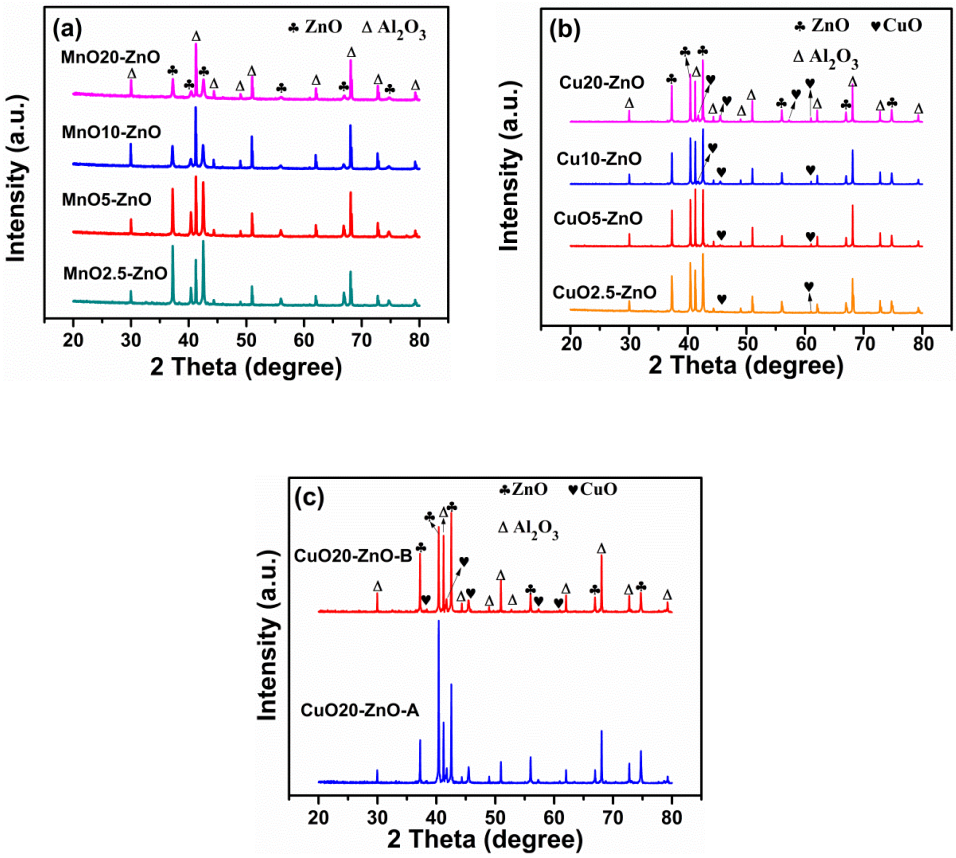

Fig. 2. XRD patterns of (a) MnO/ZnO, (b) CuO/ZnO films with different compositional ratios and (c) CuO/ZnO films from modified spraying patterns.

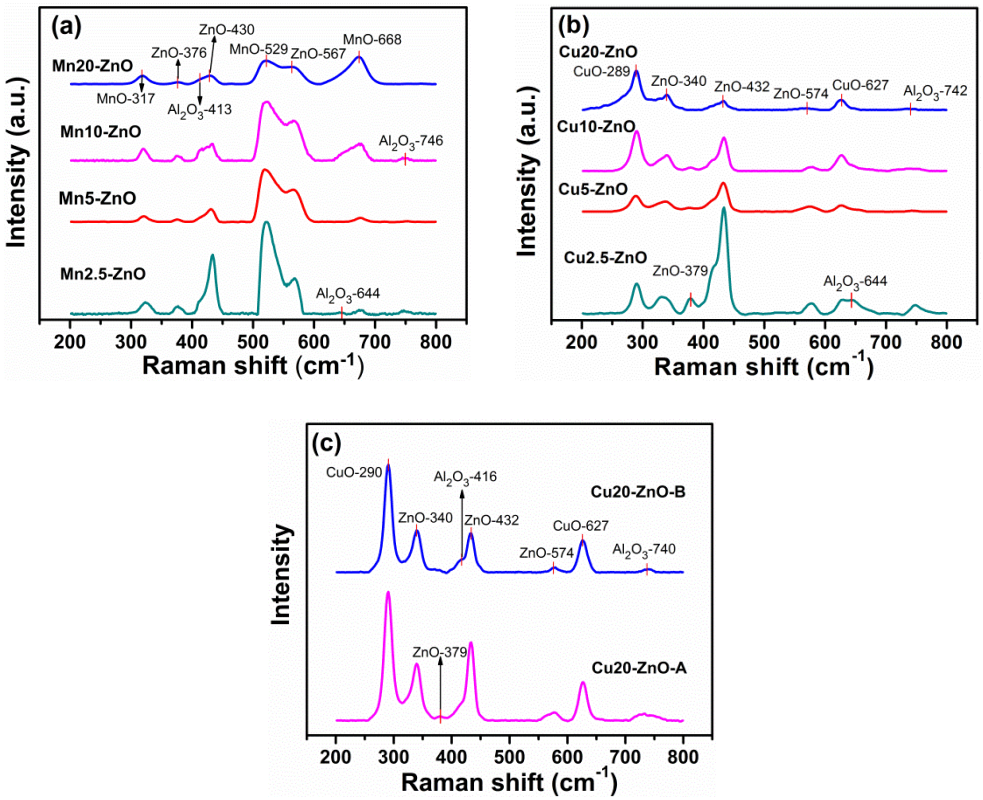

Fig. 3. Raman spectra of (a) MnO/ZnO, (b) CuO/ZnO films with different compositional ratios and (c) CuO/ZnO films from modified spraying patterns.

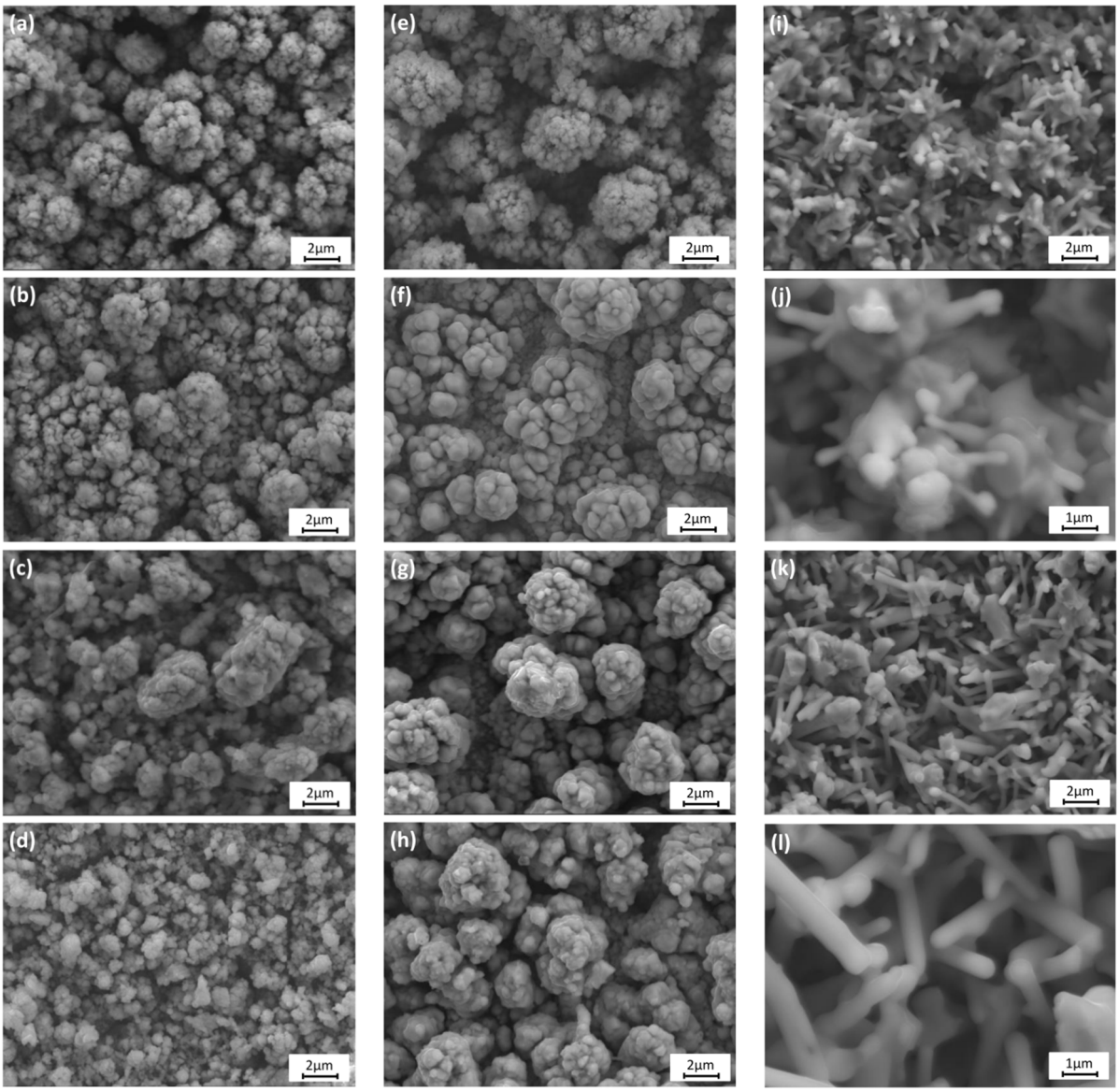

Fig. 4. Surface morphologies of (a) Mn2.5-ZnO, (b) Mn5-ZnO, (c) Mn10-ZnO, (d) Mn20-ZnO, and (e) Cu2.5-ZnO, (f) Cu5-ZnO, (g) Cu10-ZnO, (h) Cu20-ZnO and (i, j) Cu20-ZnO-A and (k, l) Cu20-ZnO-B samples.

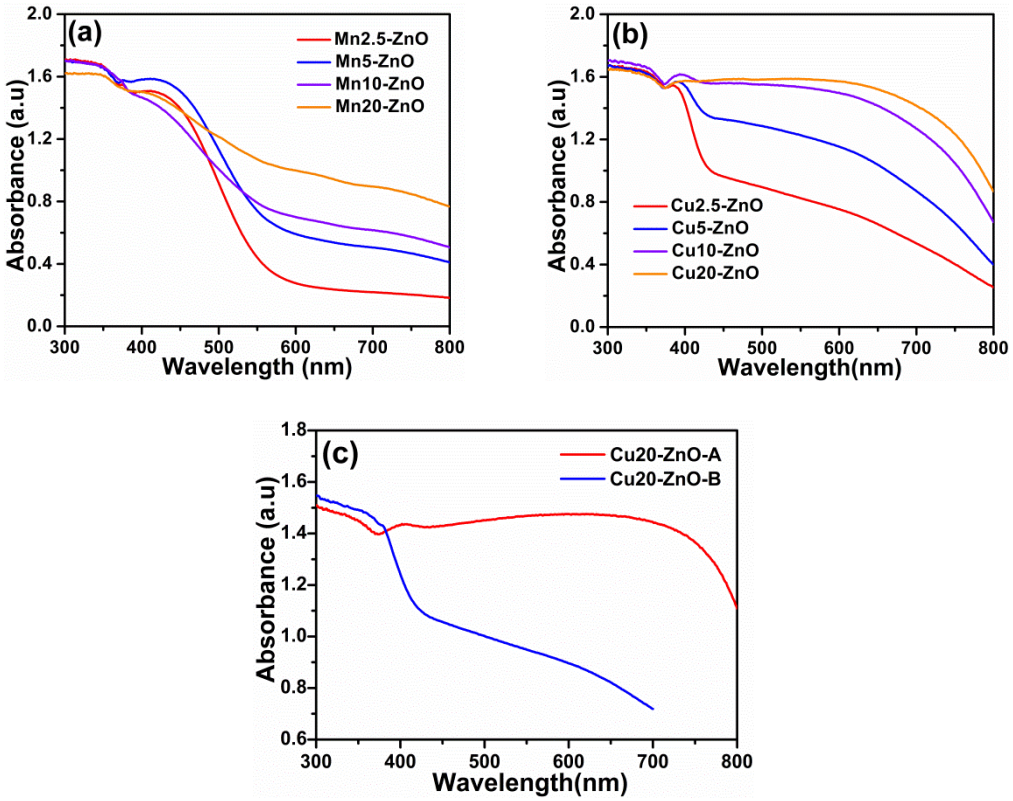

Fig. 5. UV-visible absorption spectra of (a) MnO/ZnO, (b) CuO/ZnO films with different compositional ratios and (c) CuO/ZnO films from modified spraying patterns.

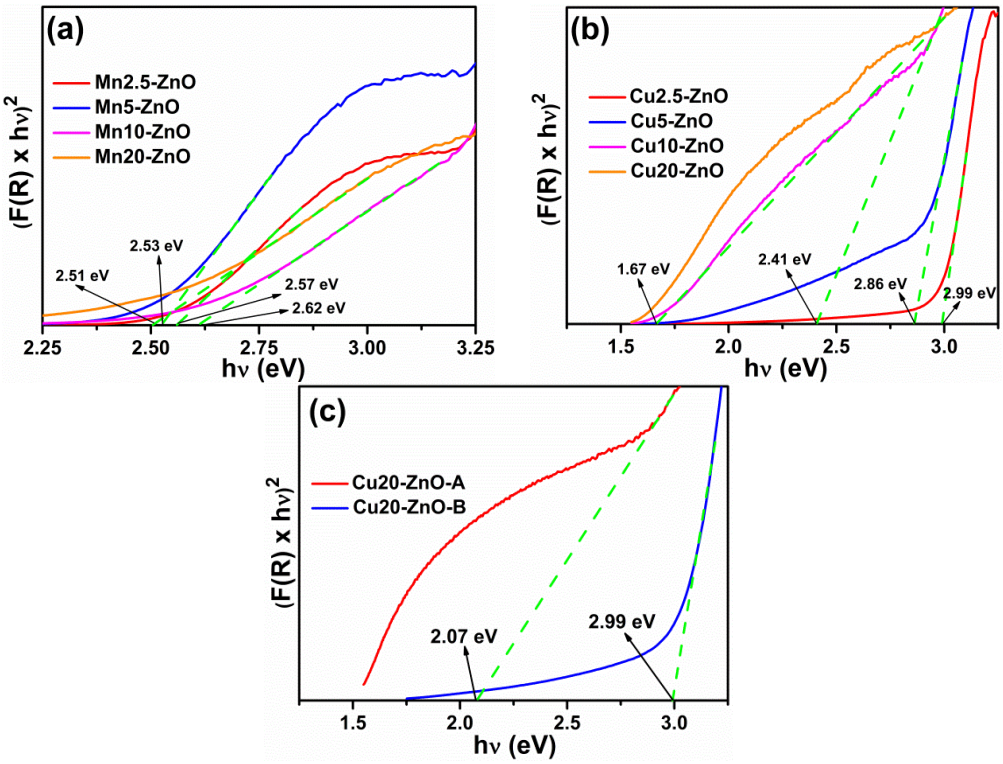

Fig. 6. Plot of $(F(R) \times h\nu)^2$ vs $h\nu$ of (a) MnO/ZnO, (b) CuO/ZnO films with different compositional ratios and (c) CuO/ZnO films from modified spraying patterns.

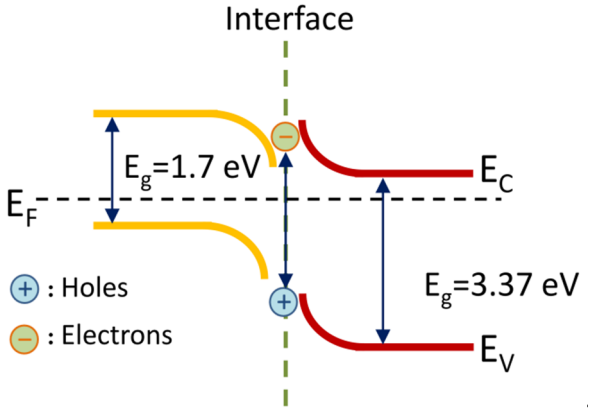

~~**Fig. 7.** Energy band diagram of CuO coupled ZnO~~

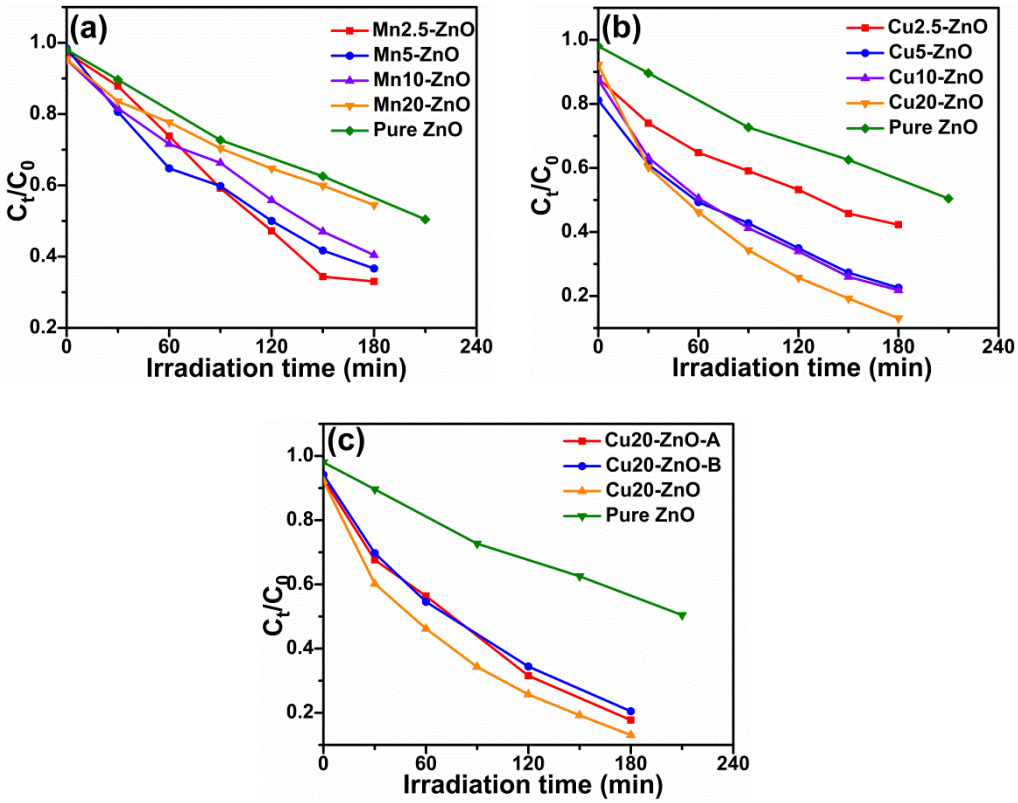

Fig. ~~8~~ 7. Photodegradation performance under UV light irradiation for the degradation of Orange II as a function of ~~irradiation~~ time for (a) MnO/ZnO and (b) CuO/ZnO films with different compositional ratios and (c) CuO/ZnO films from modified spraying patterns.

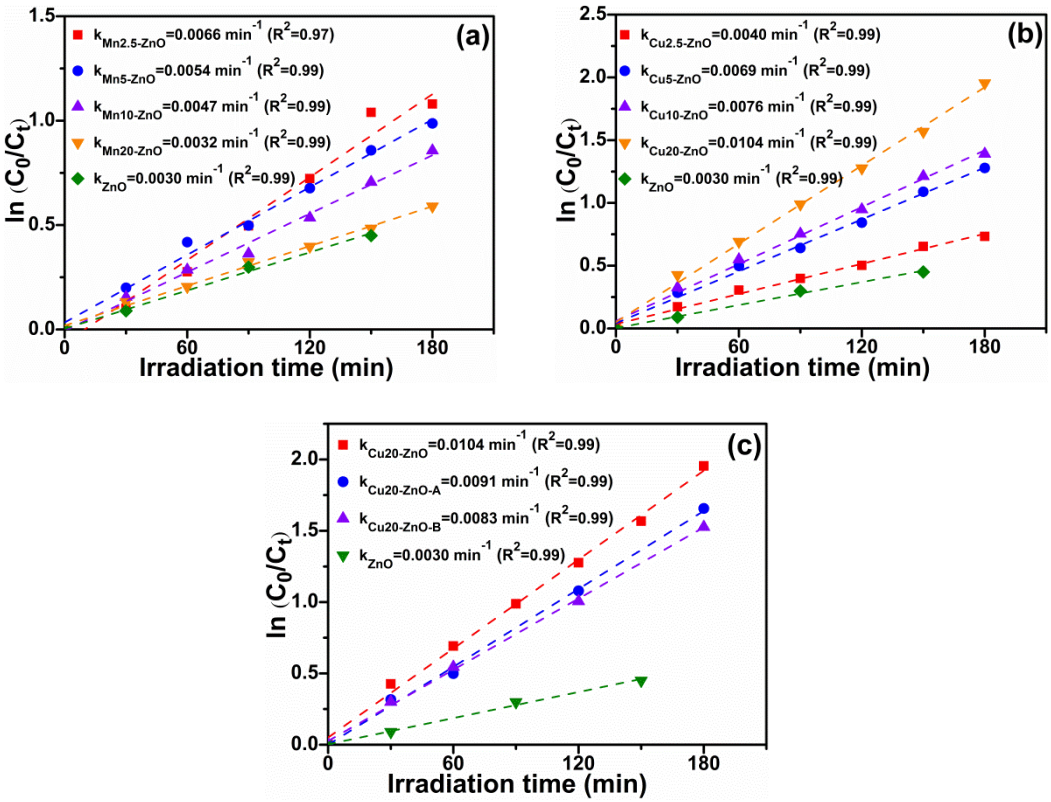

Fig. ~~9~~ 8. Plots of ln(C_0/C_t) vs. irradiation time under UV light irradiation for (a) MnO/ZnO and (b) CuO/ZnO films with different compositional ratios and (c) CuO/ZnO films from modified spraying patterns.

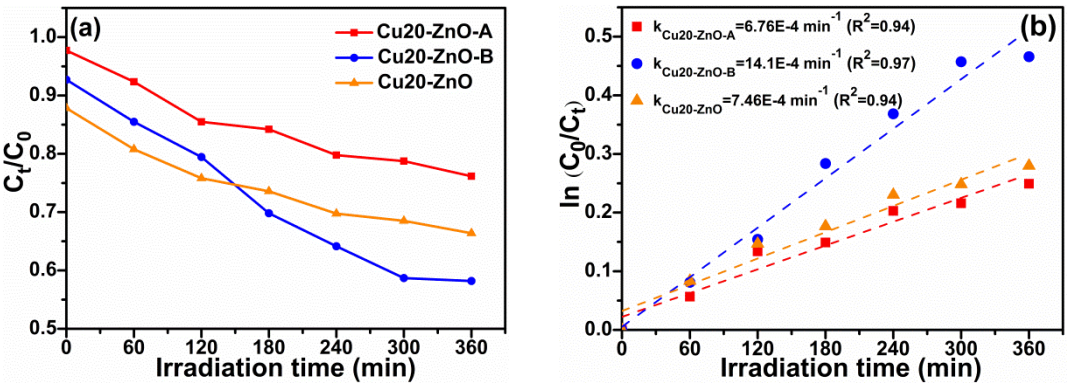

Fig. ~~10~~ 9. (a) Photodegradation performance of Orange □□~~solution~~ under visible light as a function of irradiation time for selective CuO/ZnO ~~nanocomposite~~ films ~~under visible light~~ and (b) the corresponding plots of $\ln(C_0/C_t)$ vs. irradiation time.

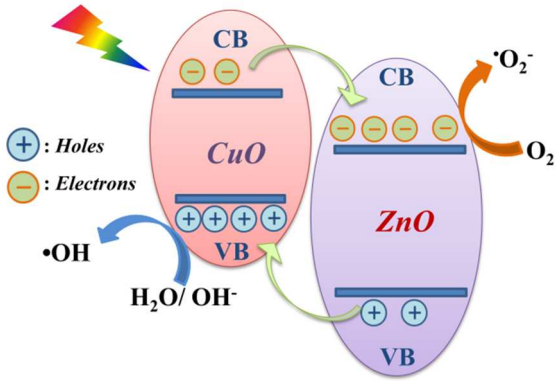

Fig. ~~11~~ 10. Schematic diagram of photodegradation mechanism for CuO/ZnO ~~nanocomposite~~ films under light irradiation.

Table 1. Solutions parameters for preparing MnO/ZnO and CuO/ZnO ~~composite~~ films

Sample name	Zinc acetate	Manganese acetate	Copper acetate	Spraying pattern
Mn2.5-ZnO	0.2 M	2.5 mol.%	0	Mixture solution
Mn5-ZnO	0.2 M	5 mol.%	0	Mixture solution
Mn10-ZnO	0.2 M	10 mol.%	0	Mixture solution
Mn20-ZnO	0.2 M	20 mol.%	0	Mixture solution
Cu2.5-ZnO	0.2 M	0	2.5 mol.%	Mixture solution
Cu5-ZnO	0.2 M	0	5 mol.%	Mixture solution
Cu10-ZnO	0.2 M	0	10 mol.%	Mixture solution
Cu20-ZnO	0.2 M	0	20 mol.%	Mixture solution
Cu20-ZnO-A	0.2 M	0	20 mol.%	Separated injection
Cu20-ZnO-B	0.2 M	0	20 mol.%	Separated injection

Table 2. Photocatalytic efficiency of CuO/ZnO heterostructured materials.

Catalyst	Pollutant	Light source	Reaction time (min)	Degradation efficiency (%)	Ref.
CuO/ZnO nano-arrays on FTO	Methylene Blue	UV	180	74	[74]
CuO-ZnO on mesh	Orange II	UV	480	88	[73]
CuO-ZnO on glass	Methylene Blue	UV	150	72	[75]
CuO/ZnO NPs	RhB	Solar	330	37.9	[76]
CuO/ZnO layer-stacked films	Orange II	UV	60	21	[77]
Cu20-ZnO films	Orange II	UV	180	88	This work

Graphical abstract